Efficient downlink MU-MIMO VLC systems with NOMA-OTFS modulation for indoor applications

Mohamed El Jbari ⓘ* and Mohamed Moussaoui
Abdelmalek Essaâdi University, National School of Applied Sciences of Tangier (ENSAT),
Information and Communication Technologies Laboratory (LabTIC), Tetuan, Morocco

ABSTRACT. In optical wireless communication (OWC), visible light communication (VLC) has shown great potential and attractive performance in indoor environments. However, the limited modulation bandwidth of VLC technologies poses performance restrictions. We propose a new approach for downlink communication utilizing multiple-input multiple-output (MIMO) technology. Our approach integrates non-orthogonal multiple access (NOMA) with orthogonal time frequency space modulation (OTFS) to improve transmission performance, particularly for low mobility when using NOMA-OTFS. Our proposed work focuses on the crucial stage of NOMA with successive interference cancellation (SIC), which involves equalization using efficient schemes, such as decision feedback equalizer (DFE), frequency-domain zero-forcing linear equalizer, and minimum mean square error-SIC at the receiver. Through extensive experimentation, it is observed that the DFE with SIC outperforms other equalizers, demonstrating a lower outage probability and a better BER. The effectiveness of the optimized analytical algorithm for ML-based downlink NOMA-OTFS modulation is confirmed through theoretical BER validation. Moreover, the simulation findings indicate that, in a multi-user (MU) scenario, the proposed NOMA-OTFS exhibits a high performance compared with traditional NOMA combined with orthogonal frequency division multiplexing in downlink MU-MIMO VLC systems. This performance advantage is observed for both MIMO and multiple-input single-output multiplexing techniques with power allocation of the users, specifically in terms of BER improvement and peak-to-average-power ratio reduction.

1 Introduction

1.1 Motivation

Researchers in the field of 6G wireless communication are increasingly interested in optical wireless communication (OWC) systems, such as visible light communication (VLC) due to its potential as a green and attractive technology for wireless communications in various environments, including indoor, vehicular, underwater, industry 4.0, and IoT applications.[1,2] VLC has demonstrated its reliability in transmitting data at high rates while providing energy-efficient, high-transmission capabilities and vast spectrum resources within the electromagnetic spectrum of 370 to 800 THz. However, the VLC channel model can be either free space or underwater,

*Address all correspondence to Mohamed El Jbari, mohamed.eljbari2@etu.uae.ac.ma

leading to an increase in channel nonlinearities that can affect system performance, requiring more complex receiver designs.[1] This becomes more challenging when there are more variables to estimate. Although standard equalizers and receivers can mitigate these impacts to some extent, the traditional modulation scheme, such as pulse-based modulation using intensity modulation detection direct (IM/DD)[3] and VLC signal processing algorithms, has limitations. In addition, the orthogonal frequency division multiplexing (OFDM) technique,[3] which can combine multiple-input and multiple-output (MIMO) transceiver schemes, faces limitations in MIMO-VLC systems due to the limited spatial diversity available in IM/DD channels. To address the small modulation bandwidth problem of light-emitting diodes (LEDs) in VLC, beyond-5G networks can utilize large-scale or massive MIMO, responsive beamforming, and non-orthogonal multiple access (NOMA) techniques to achieve high spectral efficiency (SE). MIMO is particularly effective in this context, and NOMA systems can also benefit from the high signal-to-noise ratio (SNR) available through VLC. To overcome the limited modulation bandwidth of LEDs in VLC systems, beyond 5G networks are exploring the use of large-scale or massive MIMO, responsive beamforming, and NOMA techniques.[4–8] In addition, the high SNR achievable in VLC systems is advantageous for MIMO and NOMA, especially when laser diodes (LD) and photodetectors (PD) are used in the VLC transmitter and receiver ends. Despite previous research primarily focusing on optical NOMA and multiple access (MA) schemes in VLC systems,[4,5] there is still a considerable amount of work that needs to be explored beyond what is covered in the existing literature. Currently, a novel modulation system called orthogonal time frequency space (OTFS) modulation has sparked a great deal of scientific research in radio frequency (RF)-based wireless communications[6,9] and is being investigated as a potential key component of the 6G network. OTFS has been shown to achieve superior performance compared with OFDM in both high-mobility and static channel conditions,[4,7] making it an attractive option for multi-user (MU) VLC systems[10] with less complexity. As such, there is ongoing research into the performance of OTFS compared with OFDM and NOMA schemes in indoor VLC environments. Only a few research studies[11,12] have investigated the BER performance in the downlink VLC-based NOMA-OFDMA system. Moreover, Ref. 13 has specifically focused on addressing the challenge of error propagation and enhancing both SE and data rates by employing a reconstructed hybrid optical OFDM-NOMA scheme for MU-VLC systems. It will be interesting to see how these different modulation approaches fare when applied to wireless communication using the visible light spectrum.

NOMA enables multiple users to simultaneously access the full available frequencies and bandwidth resources, resulting in higher SE improvements compared with orthogonal frequency-division multiple access (OFDMA) schemes. NOMA can be implemented using two techniques: power domain NOMA (PD-NOMA) and code division NOMA, which involves using different codes. In indoor environments, multiple LEDs are typically used to provide sufficient illumination, which has led to the adoption of MIMO designs in VLC systems. MIMO can be combined with NOMA to achieve performance targets for 6G networks, including an enhanced capacity, reliability of up to 99.999%, and reduced latency. In an MU-MIMO scenario with spatial multiplexing, the users can be grouped, with each group receiving data from a single LED. Within each group, users are overlapped in the power domain. This approach requires two levels of interference cancellation. The first level separates the MIMO subchannels, which can be achieved through transmit precoding.[8] The second level involves interference cancellation among the multiplexed users of the same LED, which can be accomplished using successive interference cancellation (SIC). Before NOMA can be adopted as a common feature in upcoming wireless networks, the challenge of developing compensation methods that effectively mitigate nonlinear distortions in high-speed MIMO VLC systems needs to be tackled. Furthermore, for future wireless networks such as UM-VLC that demand stringent quality-of-service levels, implementing NOMA poses obstacles in areas such as peak-to-average-power ratio (PAPR) reduction, downlink VLC systems, and asynchronous communications, which must be overcome. These challenges are particularly relevant for 6G networks.

The fundamental idea of OTFS is to convert the time-varying multipath channel into a two-dimensional (2D) channel in the delay-Doppler domain. By utilizing a 2D orthogonal modulation technique in the delay Doppler (DD) domain, OTFS is capable of multiplexing NM information symbols, thereby making it possible to use M Doppler bins and N delay bins. Recently,

OTFS has been studied in conjunction with a single-LED DC-biased optical (DCO) scheme for OWC, as detailed in Ref. 9. In Ref. 9, researchers investigated the use of OTFS in conjunction with a single-LED DCO scheme for OWC. In this approach, each DD domain symbol receives any time-frequency domain (TFD) channel response at an OTFS frame, enabling OTFS to access all degrees of freedom (DoF) of high-mobility channels. In addition, MIMO systems can leverage spatial DoFs to further the enhance communication reliability and rate. In conventional DD and TFD MA schemes, guard resource components are typically required. However, utilizing the additional DoFs provided by MIMO systems allows for multiple users to be supported in the spatial domain without the need for these guard resource components, as noted in Ref. 9. In addition, integrating OTFS modulation into MU-MIMO systems presents a challenge as the signals must be concurrently optimized in both the DD and spatial domains. In Ref. 10, the authors delve into the precoding design of MU m-MIMO-OTFS systems, which demand high complexity and power consumption. Furthermore, no comprehensive and concise OTFS-based MU-MIMO model for developing channel estimation, precoding, and MA schemes has been proposed. These encouraging findings emphasize the necessity for additional research into OTFS in VLC systems, which is the primary focus of this research.

In this paper, we present a new approach that combines NOMA with OTFS modulation for indoor MU-MIMO VLC systems in two scenarios: one with low mobility and the other with fast mobility. Users' mobility characteristics are considered during the simulation scenarios to implement NOMA. OTFS modulation is used in the DD plane for the high-mobility of MUs, and classical OTFS-OMA modulation is employed in the time-frequency (TF) plane to process the signals of low-mobility of MUs. Compared with NOMA-OFDM, the proposed NOMA-OTFS combination scheme offers superior SE, low PAPR, and latency reduction for both fast and slow mobile users. These advantages establish the proposed NOMA-OTFS combination scheme as a promising physical layer technique for improving the performance of future VLC systems in 6G.

1.2 Contribution of Paper

In this work, the proposed indoor MU-MIMO VLC downlink system is designed to address the demands of next-generation networks. By utilizing an MIMO VLC approach with an OTFS modulation scheme, the system can achieve a better performance compared with NOMA-OFDM VLC systems. In addition, the NOMA-OTFS technique further enhances the system's capabilities, allowing multiple users to share the same resources and optimizing the system's spectral efficiency, PAPR, BER, and latency.

The structure of this paper is organized as follows. Section 2 presents the indoor VLC system model and the fundamental principles of NOMA-OTFS, including the simple VLC channel and the NOMA-OTFS general principle. In Sec. 3, we describe the downlink NOMA-OTFS transmission for MU-MIMO VLC systems. The NOMA-OTFS detection scheme for the considered system is proposed in Sec. 4. The theoretical performance analysis, numerical results, and discussions are presented in Secs. 5 and 6. Finally, we conclude this work with a summary and future research directions in Sec. 7.

2 Indoor VLC System Model and Channel

2.1 Indoor VLC System Model

We consider an MIMO VLC scenario that uses NOMA-OTFS with two users. The system consists of two LEDs at the transmitter end and two PDs at the receiver end, located in a three-dimensional (3D) indoor room with dimensions 5 m × 5 m × 3.5 m, as shown in Fig. 1. The proposed systems employ NOMA to support u'th users, denoted as $\{U_1, U_2, U_3, \ldots, U_u\}$, $1 \leq u \leq U$, with each user being equipped with a PD. One of the LEDs either remains OFF or emits light with varying intensity based on complex OTFS modulation of the signal transmitted through the channel. The PD of the user U_u converts the optical signal to an electrical signal, which is then subjected to intensity modulation and direct detection (IM/DD) to receive the transmission data. The proposed VLC system model includes NOMA-OTFS transmission blocks that utilize two channels for data transmission, as shown in Figs. 1 and 4. The 2 × 2 transmit matrix is defined as follows:
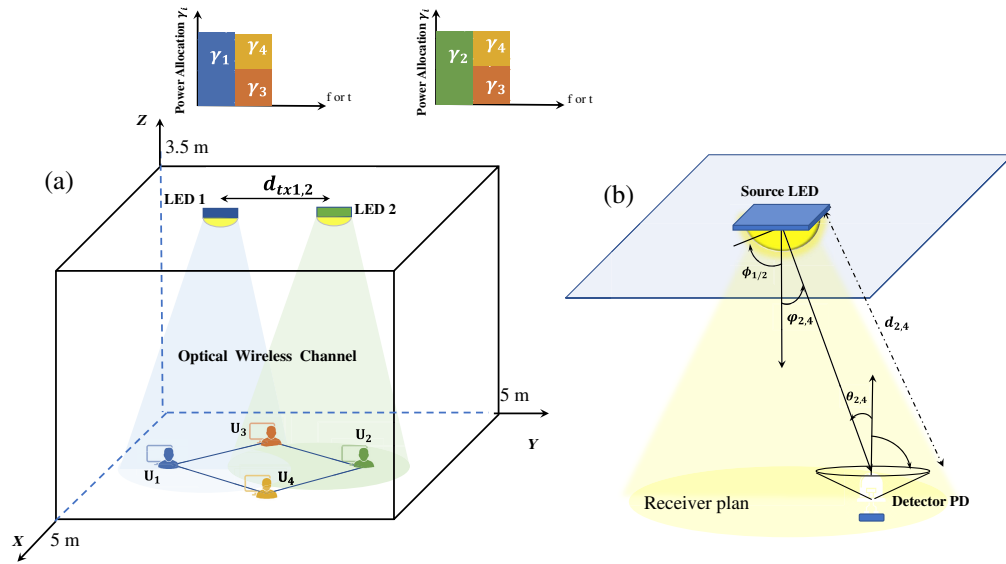
Fig. 1 Indoor scenario NOMA-OTFS model for (a) four-user VLC network with frequency or time-power allocation plane multiplexing and (b) DL of the NOMA-VLC system model.

$$X = \begin{bmatrix} x(1,1) & x(1,2) \\ x(2,1) & x(2,2) \end{bmatrix}, \tag{1}$$

where $x(N_t, q)$ represents the optical intensity transmitted through the q'th free channel using $N_t = 2$ of LEDs. Assuming a Lambertian radiation pattern, the system considers a static channel with line-of-sight (LOS) pathways connecting the LEDs and PDs. The LOS channel gain between the two LEDs and four PDs is expressed as follows:

$$h_{2,4}^{\text{LoS}} = \begin{cases} \frac{\alpha A(n+1)}{2\pi d_{2,2}^2} \cos^n(\varphi_{2,2}) g(\theta_{2,2}) \cos(\theta_{2,2}), & 0 \leq \theta_{2,2} \leq \text{FOV} \\ 0 & \theta_{2,2} > \text{FOV} \end{cases}, \tag{2}$$

where A is the PD area; α denotes the opto-electric conversion efficiency; n represents the mode number of LED Lambertian emission and is given by a function of the semi-angle $\phi_{1/2}$ at LED half power $n = \frac{-\ln(2)}{\ln(\cos \phi_{1/2})}$; $d_{2,2}$ and $\theta_{2,2}$ are the distance and the angle of incidence from second LEDs and fourth PDs, respectively; $\varphi_{2,2}$ denotes the angle of emergence from the second LED toward the second PDs; and $g(\theta_{2,2})$ represents the optical concentrator gain as follows:

$$\text{g}(\theta_{2,4}) = \begin{cases} \frac{n_r^2}{\sin^2(\text{FOV})}, & 0 \leq \theta_{2,2} \leq \text{FOV} \\ 0, & \theta_{2,2} > \text{FOV} \end{cases}, \tag{3}$$

where n_r denotes the refractive index. Considering that the receiver has excellent channel estimation and synchronization, the received matrix Y of order $N_t = 2 \times Q = 2$ is expressed as

$$Y = R_p H X + W, \tag{4}$$

where W represents the $N_t = 2 \times Q = 2$ noise matrix and R_p is the photoresponsivity of PD. However, in the considered system, the received signals are subject to the presence of noise W. This noise is modeled as an additive white Gaussian noise (AWGN) with a zero mean and a variance of σ^2. This variance is determined by the summation of the thermal noise variance σ_{th}^2 and the shot noise variance σ_{sh}^2, which are computed according to Ref. 14. The average SNR is written as

$$\text{SNR} = \frac{\mathcal{R}_p^2}{4\sigma^2} \sum_{i=1}^{N_r=2} \mathbb{E}[|h_i X|^2], \tag{5}$$

where h_i is the i'th row of the H matrix.

2.2 VLC Channel

Consider a downlink NOMA-OTFs MUs 2×2-MIMO VLC system with two LEDs located in the center of the indoor room dimension and four Us associated by their PDs as shown in Fig. 1.

2.3 NOMA-OTFS-Based MU-VLC Principle

NOMA-OTFS is a communication technique that aims to improve spectral efficiency by exploiting the TF plane and the delay-Doppler (DD) plane efficiently, as shown in Fig. 3. The underlying principle is to allocate different power levels to different users in the DD plane, while exploiting the TF plane to achieve orthogonal signaling. This allows multiple users to transmit the data on the same channel simultaneously, without interfering with each other. A discrete TF plane can be obtained by sampling at regular intervals of T (s) and Δf (Hz). In this discretized representation, the TF domain resource is represented as $N \times M$ point arrays:

$$\Lambda_{\text{TF}} = \{(nT, m\Delta f), \, n = 0. \ldots \ldots N - 1; \, m = \ldots, 2, \ldots M - 1\}. \tag{6}$$

The corresponding discrete DD domain is obtained by TF converted using a 2D simplistic Fourier transform as follows:

$$\Gamma_{\text{DD}} = \left\{ \left(\frac{k}{NT}, \frac{l}{M\Delta f} \right), k = 0,1, \ldots N - 1; l = 0,1,2, \ldots, M - 1 \right\}. \tag{7}$$

The parameters N and M represent the number of time slots and samples per block, respectively, in both the TF and DD domains. Meanwhile, the values of $\frac{1}{NT}$ and $\frac{1}{M\Delta f}$, which are determined by the channel characteristics, define the path delay and Doppler shift resolution, respectively.

The underlying concept of the NOMA-OTFS techniques is to exploit the TF and DD domains simultaneously. MUs with different mobility profiles are clustered together and served concurrently in the TF domain. However, for highly mobile users, their signals are allocated with time-invariant channel gains in the DD domain, which requires both N and M to be large. This presents a challenge in OMA-OTFS as each frequency channel $M\Delta f$ is occupied for a long duration NT by highly mobile users, even when the channel conditions are weak. As a result, using the NOMA-OTFS scheme enables bandwidth sharing and ensures that the signals of highly mobile users can be spread across multiple TF resources without reducing SE. Meanwhile, the signals of low-mobility users are managed in the TF domain. The NOMA technique effectively manages interference from users with different mobility profiles. Upon comparing OMA-OTFS and NOMA-OTFS, it has been observed that the latter technique enhances the overall SE and optimizes the utilization of bandwidth resources for highly mobile users.

Figure 1 shows the proposed NOMA-OTFS-based MIMO VLC network, which comprises two LEDs and four PDs at the receiver. Specifically, the network includes two optical cells and four users (Us) located in different positions within an indoor room, as shown in Fig. 1(b). In this scenario, the Us numbered U_1 and U_2 are in the non-overlapping areas served by the LEDs of their cells. However, the U_1 and U_2 are multiplexed in the power domain. In the overlapping region, there are two users U_3 and U_4. These users are illuminated by two LEDs and receive superimposed optical signals transmitted by these LEDs. The LEDs utilize the bandwidth in the blue and green cells. To mitigate interference, sufficient bandwidth has been appropriately allocated.

3 Downlink NOMA-OTFS Transmission for MU-MIMO VLC System

This section focuses on the MIMO downlink NOMA-OTFS transmission, in which the pre-and post-processing block diagram of the OTFS modulation involves 2D inverse symplectic finite Fourier transforms (ISFFTs). The ISFFT is performed at the NOMA-OTFS transmitter, which employs two LEDs as shown in Figs. 1(a) and 2. The NM data information symbols $x[k, l]$, $l = 1, \ldots .N - 1$, $l = 0,1, \ldots M - 1$ are multiplexed on a DD domain matrix X_{tn} of size $N \times M$. $x[k, l] \in A$ (i.e., conventional modulation alphabet as QAM, BPSK) are converted into a TF domain matrix $X[n, m]$ using the ISFFT in 2D $N \times M$-point as follows:[6]
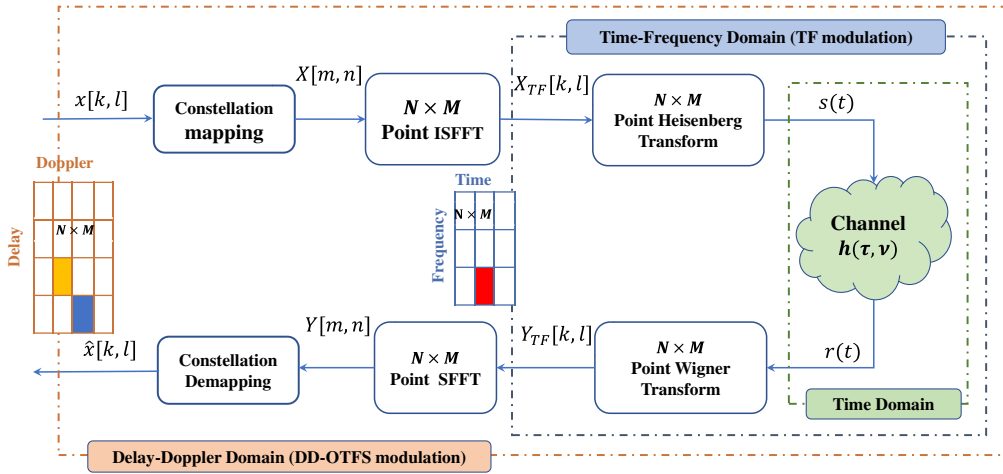
Fig. 2 Block diagram of the OTFS modulation/demodulation scheme.

$$X[n,m] = \frac{1}{NM}\sum_{k=0}^{N-1}\sum_{l=0}^{M-1} x[k,l]e^{j2\pi-\left(\frac{nk}{N}-\frac{ml}{M}\right)}, \qquad (8)$$

where $n \in \{0,1,2,\ldots,N-1\}$ and $m \in \{0,1,2,\ldots,M-1\}$. The NOMA technique is used to address the signals from users (Us) with different mobility profiles in the TF domain. As shown in Fig. 4, each K-NOMA opportunistic user selects the M'th Us, where $K \geq M$. Each NOMA-Us with low mobility receives N information data-bearing $x_u(n)$ symbols occupying one frequency subchannel. The TF signal transmitted by LEDs to users with low mobility is mapped to NM modulation symbols from a conventional alphabet A using the following expression:

$$X_u[n,m] = \begin{cases} x_u(n) & \text{if } m = u-1 \\ 0 & \text{otherwise} \end{cases}, \quad \text{with } 1 \leq u \leq M \text{ and } 0 \leq n \leq N-1. \qquad (9)$$

The LEDs superimpose high-mobility Us TF signals between the low-mobility NOMA-Us signals as

$$X[n,m] = \gamma_0 X_0[n,m] + \sum_{u=1}^{M} \gamma_u X_u[n,m], \qquad (10)$$

where $\sum_{u=1}^{M} \gamma_u^2 = 1$ for the γ_u coefficient of the NOMA allocation of the u'th Us.

The LED transmitter signal is generated by converting the complex matrix $X[n,m]$ in the TF domain to TD matrix S. This is achieved by applying the M-point Heisenberg transform using the inverse discrete Fourier transform (IDFT). The TD signal transmitted by the LED is represented by the following expression:

$$s(t) = \sum_{n=0}^{N-1}\sum_{m=0}^{M-1} X[n,m]p_{tx}(t-nT)e^{j2-m\Delta f(t-nT)}, \qquad (11)$$

where $p_{tx}(t)$ is the transmitter pulse shaping waveform. After performing the Heisenberg transform, i.e. the parallel to serial (P/S) conversion is applied and the real part is split from the imaginary part. This is followed by switching, digital to analog conversion, and the addition of a direct current (DC) bias. The resulting time-domain signals, $s(t)$, are then transmitted using LED technology over VLC channels, as depicted in Figs. 2–4.

4 MU-MIMO VLC System Using NOMA-OTFS Detection

4.1 OTFS Demodulation

The receiver comprises PDs for each U, which detect the TD signal $s(t)$ transmitted through a time-varying channel with a complex baseband that is delayed in time τ and shifted in frequency ν.
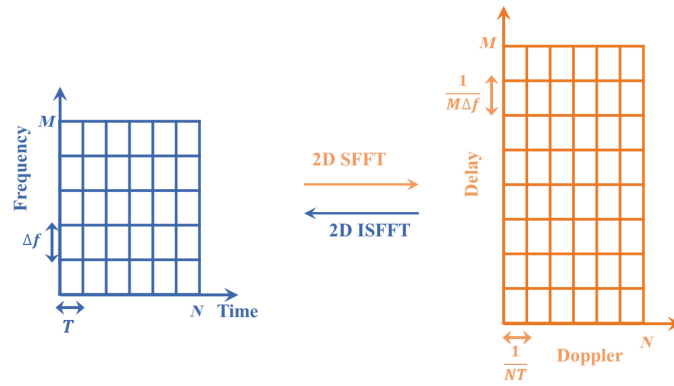
Fig. 3 Discrete TF Λ_{TF} and delay-Doppler Γ_{DD} grids.
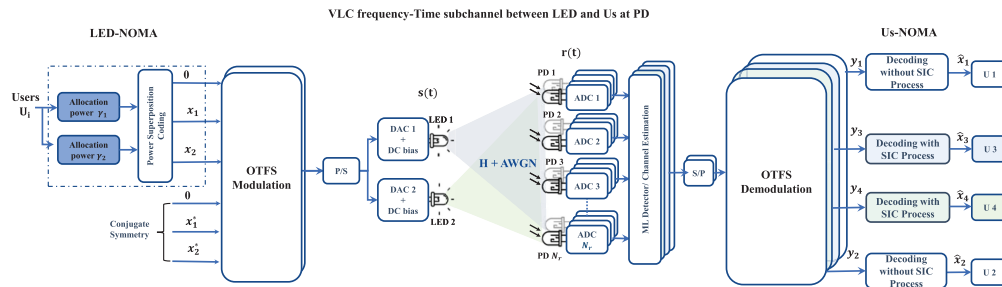

Fig. 4 Block diagram of the downlink NOMA-OTFS VLC system.

The channel response is denoted as $h_u(\tau, \nu)$. The received signal at each user u in the TD is expressed as follows:

$$r_u(t) = \iint h_u(\tau, \nu)s(t-\tau)e^{j2\pi\nu(t-\nu)}\mathrm{d}\tau\,\mathrm{d}\nu + v(t), \tag{12a}$$

where $v(t)$ represents the additive noise at the receiver. The expression of $h_u(\tau, \nu)$ is defined as follows:

$$h_u(\tau, \nu) = \sum_{p=0}^{P_u} h_{u,p}\delta(\tau - \tau_{u,p})\delta(\nu - \nu_{u,p}), \tag{12b}$$

where $\tau_{u,p}$ and $\nu_{u,p}$ represent the time delay and shifting Doppler of the p'th propagation path, respectively. These parameters are functions of the discrete delay $l_{\tau_u,p}$, Doppler tap index $k_{\nu_u,p}$, fractional delay $\tilde{l}_{\tau_u,p}$, and shifting Doppler $\tilde{k}_{\nu_u,p}$. $h_{u,p}$ corresponds to the channel gain associated with the p'th propagation path. The expressions for $\tau_{u,p}$ and $\nu_{u,p}$ are given as follows:

$$\tau_{u,p} = \frac{l_{\tau_u,p} + \tilde{l}_{\tau_u,p}}{M\Delta f}, \quad \nu_{u,p} = \frac{k_{\nu_u,p} + \tilde{k}_{\nu_u,p}}{NT}. \tag{13}$$

The channels of low mobility NOMA users do not experience shifting Doppler. However, their channels are represented as

$$h_u(\tau, \nu) = \sum_{p=0}^{P_u} h_{u,p}\delta(\tau - \tau_{u,p}), \quad \text{for } 0 \leq u \leq K. \tag{14}$$

Following the PD detection, ADC, and DC removal, the time-domain signal is processed by the maximum likelihood (ML) detector and then subjected to serial to parallel (S/P) conversion. The resulting time-domain signal at each user u is then transformed into a TF signal using the $N \times M$-point Wigner transform as follows:

$$Y_u[n, m] = H_u[n, m]X[n, m] + W_u[n, m] = Y_u(t, f)|_{(t=nT, f=m\Delta f)}. \tag{15a}$$

The cross-ambiguity function, denoted as $Y_u(t, f)$, is computed using the matched filter and is expressed as follows:

$$Y_u(t, f) = \int r_u(t) p_{rx}^*(t' - nT) e^{j2\pi m \Delta f(t' - nT)} dt', \tag{15b}$$

where $W_u[n, m]$ is the Gaussian noise matrix in the TF plane, $p_{rx}(t)$ represents the pulse shaping waveform at the receiver, and $H_u[n, m] = \iint h_u(\tau, \nu) e^{j2\pi \nu nT} e^{-j2\pi(\nu + m\Delta f)\tau} d\tau \, d\nu$ denotes the effective channel matrix in the TF plane.

In the proposed downlink NOMA-OTFS scheme, direct detection of User U_u's signals in the DD plane is achieved by considering NOMA users' signals as noise. This is accomplished by applying the SFFT to the received signal $Y_u[n, m]$ to obtain the DD estimates as follows

$$
\begin{aligned}
Y_u[n, m] &= \frac{1}{NM} \sum_{n=0}^{N-1} \sum_{m=0}^{M-1} Y_u[n, m] e^{-j2\pi \left(\frac{nk}{N} - \frac{ml}{M}\right)} \\
&= \frac{1}{NM} \sum_{q=0}^{M} \gamma_q \sum_{n=0}^{N-1} \sum_{m=0}^{M-1} x_q[n, m] h_{\omega, u} \left(\frac{k-n}{NT}, \frac{l-m}{M\Delta f}\right) + z_u[k, l],
\end{aligned}
\tag{16}
$$

where $x_q[n, m]$ is the DD representation of $X_q[n, m]$ for the q user index and $h_{\omega, u}$ denotes the circular convolution channel response with a windowing function $w(\tau, \nu)$.[10] In NOMA-OTFS, for detecting the signals of high mobility Us, the relationship between the transmitted signals and the observations in the DD domain is expressed using the channel model in Eq. (15) as follows:

$$y_u[k, l] = \sum_{q=0}^{M} \gamma_q \sum_{p=0}^{P_u} h_{u,p} x_q[(k - k_{\nu_i, p})_N, (l - l_{\nu_i, p})_M] + z_u[k, l], \quad \text{if } N \text{ and } M \text{ are sufficient,} \tag{17}$$

where $((.))_M$ represents the modulo M operator. The effect of delay or Doppler fraction $\tilde{l}_{\tau_u, p} = \tilde{k}_{\nu_i, p} = 0$ on the inter-Doppler interference. In OMA-OTFS, increasing the values of N and M can lead to a significant reduction in SE due to the increase in the number of subcarriers and time slots required for each U. However, in NOMA-OTFS, the use of large N and M becomes possible because of the ability to share the same spectrum among MUs with different mobility profiles. We use Eq. (17) for detecting downlink NOMA-OTFS in Sec. 4.2; it can be vectorized as[11,15]

$$y_u = \mathcal{R}_p \gamma_0 H_u S_u + W_u = \mathcal{R}_p \gamma_0 H_u S_u + \sum_{q=1}^{M} \mathcal{R}_p \gamma_q H_u x_{q,n} + z_{u,n}, \tag{18}$$

where $y_u, S_u \in C^{N_r \times NM}$ are the received and the transmit signals matrices. Then the AWGN vectors $z_u \in C^{N_r \times NM}$ and $H_u \in C^{NM \times NM}$ denote the 2×2-MIMO VLC channel matrices corresponding to W_u interference and noise matrix terms, respectively.

4.2 NOMA-OTFS Detection for MU in 2 × 2-MIMO-VLC Systems

The SIC algorithm is a popular technique used in NOMA systems to separate the signals from different users. The first stage of the SIC algorithm involves decoding the signal of the NOMA user with the highest power level in the DD plane. This decoded signal is then subtracted from the received signal to remove its contribution from the signal of other users. The process is repeated until all users have been decoded in the DD plane. In the second stage of the SIC algorithm, the signals of each NOMA user are separated in the TF plane. The signal of the NOMA user with the highest power level is first decoded in the TF plane, followed by the decoding of signals from other users in decreasing order of their power levels. After the signals from all NOMA users have been separated and decoded in both the DD and TF planes, the original transmitted data can be recovered through QAM demodulation. This section describes in detail the two stages of the SIC algorithm used in Algorithm 1 to achieve this operation.

Algorithm 1 Proposed algorithm for NOMA-OTFS downlink equalization

---

1. Input: $\mathbf{U_i}$ users, channel matrix $\mathbf{H_{U_i}}$, the received symbol vector $\mathbf{y_u}$, the power allocation powers $\gamma_1, \gamma_2, \gamma_3, \gamma_4$

2. Initialize: Detecting symbol $\mathbf{D_u}$, $\mathbf{Y_m^u} = \mathbf{y_{u,1}}$, $\hat{\mathbf{x}}_1 = \hat{\mathbf{x}}_2 = \mathbf{x_{q,1}} = \mathbf{x_{q,2}} = \mathbf{x_{q,3}} = \mathbf{x_{q,4}} = 0_{\mathbf{M \times N \times N_t}}^{\mathbf{u}}$

3. Define $\mathbf{D_u} = \{0, , 2, \ldots. \mathbf{N} - 1\}$, $\mathbf{D_1} = \varnothing$

4. For $\mathbf{u} = 1$ **to** 4

5. Transmit the corresponding symbol of each user applying NOMA-OTFS [Eqs. (8)–(11)].

6. Detect the received symbol from four users through OTFS demodulation [Eqs. (12)–(16)].

7. Decode directly $\mathbf{U}_1$ and $\mathbf{U}_2$ without SIC processing.

8. Decode $\mathbf{U}_3$ and $\mathbf{U}_4$ with NOMA-SIC in two steps [Eqs. (19)–(38)].

    i.   Equalize DD domain signals of $\mathbf{U}_3$ and $\mathbf{U}_4$ using FD-ZFLE or DFE equalizers.

    ii.   Detect and remove the NOMA user's signal from $\mathbf{U}_3$ and $\mathbf{U}_4$ at the receiver.

9. Calculate outage probability, $\mathbf{P_{out}}$, using either the ZF or DFE equalizer.

10. Choose downlink users' symbol rate sets.

11. $\{\mathbf{n} \in \mathbf{D_u}; \hat{\mathbf{x}}_\mathbf{u}[\mathbf{n}]\}$, $\forall \mathbf{u} \in \{1, .., 4\}$

12. Detect symbol data equalizer in output vectors.

13. $\hat{\mathbf{x}}_\mathbf{u}(\mathbf{n})$, $\forall \mathbf{u} \in \{1, .., 4\}$

14. Rest $\mathbf{x_{q,1}} = 0$, $\mathbf{x_{q,2}} = 0$, $\mathbf{x_{q,3}} = 0$, and $\mathbf{x_{q,4}} = 0$.

15. Compute the PEP using ML [Eq. (43)].

16. If $\mathbf{D_u} = \varnothing$, pause.

17. End

18. Output: Equalized data symbol of $\hat{\mathbf{x}}_\mathbf{u}$.

4.2.1 First stage of NOMA-SIC

Assume a downlink MU 2×2-MIMO VLC system with four receiving PDs supporting four users, in which each LED transmits four independent data streams. On the receiver side, there are four receiving PDs, each corresponding to one of the four users. The received signal vector $Y_i \in C^{N_r \times NM}$ at each PD is expressed as follows:

$$Y_u = \mathcal{R}_p \gamma_0 H_u S_u + \sum_{u=1}^{U-1} \sum_{q=1}^{M} \mathcal{R}_p \gamma_q H_u x_{q,n} + \eta_u, \tag{19}$$

where H_u and $S_u \in C^{N_r \times NM}$ are the convolution matrix, and the stacking converted time-plane signal vector, respectively, for user U, and η_u denotes the AWGN vectors. The channel impulse response matrix $H_u^{N_t, N_r} \in C^{M \times M}$ between the $N_t = 2$ transmitter element and $N_r = 2$ receiver for the i'th symbol is defined as follows:

$$H_u = \begin{bmatrix} H_i^{0,0} & H_i^{0,1} & \cdots & H_i^{0,N_t-1} \\ H_i^{1,0} & H_i^{1,1} & \cdots & H_i^{1,N_t-1} \\ \vdots & \vdots & \ddots & \vdots \\ H_i^{N_r-1,0} & H_i^{N_r-1,1} & \cdots & H_i^{N_r-1,N_t-1} \end{bmatrix}, \tag{20}$$

where $H_i^{N_t, N_r}$ represents the submatrix structure, i.e., the circulant matrix is determined by the channel response $y[k, l]$ in Eq. (17). We note that the diagonalization of an $N_t \times N_r$ circulant matrix uses the $N_t \times N_r$ discrete Fourier transform (DFT) F_N and IDFT F_N^{-1}. For the H_i^u structure matrix, the inter-symbol interference (ISI) still must be considered in NOMA-OTFS for the VLC

system. Therefore, the key idea is to equalize the $N_t \times N_r$-MIMO applying two methods: the frequency-domain zero-forcing linear equalizer (FD-ZFLE) and the decision feedback equalizer (DFE).

FD-ZFLE equalizer. The FD-ZFLE equalizer consists of two steps. In the first step, we multiply the observation vector Y_i in Eq. (19) by the matrix $F_N \otimes F_N^H$, where $\otimes$ is the Kronecker product. Then, the received signals for NOMA-OTFS transmission are expressed as

After the OTFS demodulation, the TF received signal for NOMA-OTFS transmission at the PDs for the i'th NOMA symbol is expressed as

$$\tilde{Y}_i = D_i(F_N \otimes F_M^H)\left[\mathcal{R}_p \sum_{u=0}^{U-1}\left(\gamma_0 S_u + \sum_{q=1}^{M} \gamma_q x_{q,n}\right)\right] + \tilde{\eta}_u, \tag{21}$$

D_u denotes the $NM \times NM$ diagonal matrix, where the $(kM + l + 1)$'th diagonal element is determined by the following expression:

$$D_u^{(k,l)} = \sum_{n=0}^{N-1} \sum_{m=0}^{M-1} A_{0,n}^{m,1} e^{j2\pi \frac{lm}{M}} e^{-j2\pi \frac{kn}{N}}. \tag{22}$$

$A_{0,n}^{m,1}$ is the element located in the $(nM + m + 1)$'th row and the first column of H_u, and $\tilde{\eta}_u = (F_N \otimes F_N^H)\eta_u$. The FD channel matrix for Us is represented as

$$\tilde{H}_{\text{FD},i}^U = D_i(F_N \otimes F_M^H)\tilde{H}_i^U. \tag{23}$$

where

$$\tilde{H}_i^u = \begin{bmatrix} H_0^u & 0_{M\times N}^u & \cdots & 0_{M\times N}^u \\ 0_{M\times N}^u & H_1^u & \cdots & 0_{M\times N}^u \\ \vdots & \vdots & \ddots & \vdots \\ 0_{M\times N}^u & 0_{M\times N}^u & \cdots & H_{N-1}^u \end{bmatrix}. \tag{24}$$

Let $\tilde{H}_{\text{FD}i,m}^U \in C^{MN_r \times MN_t}$ be the FD matrix for Us, the i'th NOMA user, and the m'th subcarrier, which is constructed by the $(M - 1)$'th element row-wise stacking and column-wise from $\tilde{H}_{\text{FD},i}^U$ for $m = 0, \ldots, M - 1$.

Considering that two LEDs at the transmitter end are equipped with four Us at the receiving PDs, the matrix $\ddot{H}_{u,m} \in C^{N_r \times (N_t \times U)}$ is constructed by $\tilde{H}_{\text{FD}i,m}^U$ for each U, which is applied in the ZFE equalization process. Because the $\ddot{H}_{u,m}$ matrix is given as

$$\ddot{H}_{u,m} = \begin{bmatrix} \tilde{h}_{(0,0);u,m}^0 & \tilde{h}_{(0,0);u,m}^1 & \tilde{h}_{(0,1);u,m}^0 & \tilde{h}_{(0,1);u,m}^1 \\ \vdots & \vdots & \vdots & \vdots \\ \tilde{h}_{(N_r-1,0);u,m}^0 & \tilde{h}_{(N_r-1,0);u,m}^1 & \tilde{h}_{(N_r-1,1);u,m}^0 & \tilde{h}_{(N_r-1,1);u,m}^1 \end{bmatrix}, \tag{25}$$

where $\tilde{h}_{(N_r,N_t);u,m}^u$ denotes the FD matrix coefficient and N_r and N_t are the transmitter and receiver for Us, respectively. Assuming the ZFE equalization approach, we express the equalized signal Y_i as

$$Y_{u,m} = (\ddot{H}_{u,m})^+ Y_{u,m}, \tag{26}$$

where $Y_{u,m} \in C^{N_r \times 1}$ is the receiver TF signal vector. $Y_{u,m}$ is constructed by taking the equalized signal $\tilde{y}_{(N_t);u,m}^u$ from the N_t transmitter of user u. The expression of $Y_{u,m}$ for i'th symbol and m'th subcarrier can be given as

$$Y_{u,m} = \begin{bmatrix} \tilde{y}^0_{(0);i,m} \\ \tilde{y}^1_{(0);i,m} \\ \tilde{y}^0_{(1);i,m} \\ \tilde{y}^1_{(1);i,m} \end{bmatrix}. \tag{27}$$

The second step is to apply the $(F_N \otimes F_N^H)^{-1}D_u^{-1}$ to $\tilde{Y}_u$; then the received Us signal expression is given as

$$Y_u = \mathcal{R}_{\mathrm{p}} \sum_{u=0}^{U-1} \left(\gamma_0 S_u + \sum_{q=1}^{M} \gamma_q x_{q,n} \right) + (F_N \otimes F_M^H)^{-1}D_u^{-1}\tilde{\eta}_u, \tag{28}$$

$$Y_u = \mathcal{R}_{\mathrm{p}} \left(\gamma_u S_u + \sum_{\substack{q=1 \\ q \neq u}}^{M} \gamma_q x_{q,n} \right) + (F_N \otimes F_M^H)^{-1}D_u^{-1}\tilde{\eta}_u, \tag{29}$$

where $\hat{Y}^u_{u,m} \in C^{NMN_r \times 1}$ is the TF vector signal of each user, which is estimated by the DD plane, and their transmitted vector is obtained as

$$\hat{X}^u = (F_N \otimes I_{N_t} \otimes F_M^H)\hat{Y}^u_{u,m}. \tag{30}$$

To calculate the signal to interference and noise ratio (SINR) of the u'th user at PDs for detecting all $x[k, l]$, the following expressions is utilized as

$$\mathrm{SINR}^{\mathrm{LE}}_{u,kl} = \frac{\mathrm{SNR}\gamma_u^2}{\mathrm{SNR}\gamma_1^2 + \frac{1}{NM} \sum_{\tilde{k}}^{N-1} \sum_{\tilde{l}}^{M-1} |D_u^{\tilde{k},\tilde{l}}|^{-2}}. \tag{31}$$

DFE equalizer. At the heart of DFE lies the concept of utilizing previously detected symbols to provide feedback. By incorporating this feedback, DFE can mitigate the ISI effects and improve the overall performance of the system. The initial stage entails the retrieval of the signal vectors that were received in Eq. (19): $Y = \mathcal{R}_{\mathrm{p}}\gamma_0 \sum_{u=0}^{U-1} \gamma_0 S_u + \sum_{u=0}^{U-1} \sum_{q=1}^{M} \mathcal{R}_{\mathrm{p}}\gamma_q x_{q,n}$. The signal vectors are processed using the DFE equalizer to generate the outputs of the system, which are defined as

$$\hat{y} = P_u Y_u - G_u \check{y}, \tag{32}$$

where $\check{y}$ is the decision made on the symbols, $P_u = L_u(H_u^H H_u)^{-1}H_u^H$ denotes the DFE-forward part of the equalizer, and $G_u = L_u - I_{NM}$ represents the feedback part of DFE with L_u denoting the low triangular matrix, which is calculated by the Cholesky decomposition of H_u. The detected Us signals are expressed as follows:

$$\hat{y} = \mathcal{R}_p \gamma_0 H_u S_u + \underbrace{\sum_{u=1}^{U-1} \sum_{q=1}^{M} \mathcal{R}_p \gamma_q x_{q,n} + L_u(H_u^H H_u)^{-1}H_u^H \eta_u}_{\text{Interference and noise terms (IN)}}. \tag{33}$$

The covariance matrix for SINR is expressed as

$$C_{\mathrm{cov}} = \mathrm{SNR}\gamma_1^2 I_{MN} + L_u(H_u^H H_u)^{-1}H_u^H. \tag{34}$$

Hence, the achieving SINR of DFE required to detect the $x[k, l]$ detector is given as

$$\mathrm{SINR}^{\mathrm{DFE}}_{u,kl} = \frac{\mathrm{SNR}\gamma_u^2}{\mathrm{SNR}\gamma_1^2 + A_{u,kl}^{-1}}, \tag{35}$$

where $A_{u,kl}$ is the $(kM + l + 1)$'th element of the diagonal matrix A_i, which is obtained by the Cholesky decomposition as

$$A_{u,(N-1)(M-1)} = \sum_{p=0}^{P_0} |h_{u,p}|^2. \tag{36}$$

4.2.2 *Second stage of NOMA-SIC*

Assuming the high mobility of Us, NM signals are effectively decoded, deleted, and removed using the FD-ZFLE or DFE equalization techniques; then the mapping scheme for NOMA-Us detection in the TF domain is expressed as

$$Y_u[n,m] = \sum_{u=0}^{U-1} \sum_{q=1}^{M} \gamma_q H_u[n,m] X_q[n,m] + W_i[n,m] = \sum_{u=0}^{U-1} \gamma_1 H_u[n,m] x_{m+1}(n) + W_u[n,m]. \tag{37}$$

Let us assume that the low-mobility user U_u is exclusively interested in $Y_u[n, u-1]$ for $0 \le n \le N-1$ and all NOMA-Us use the same power allocation. Then, the detected information data signal is expressed by applying equalization to Eq. (37) as

$$\hat{x}_u(n) = \frac{Y_u[n, u-1]}{\gamma_1 H_u[n, u-1]}. \tag{38}$$

This implies that the SNR for detecting $\hat{x}_u(n)$ is calculated as

$$\mathrm{SNR}_{u,n} = \mathrm{SNR} \gamma_1 |H_u[n, i-1]|^2. \tag{39}$$

The outage probability P_{out} for $x_u(n)$ when applying the FD-ZFLE or DFE equalization in the first stage of the SIC is given as

$$\mathcal{P}_{\mathrm{out}}(\mathrm{SNR}_{u,n}, \mathrm{SINR}_{u,kl}) = \begin{cases} 1 - p(\mathrm{SNR}_{u,n} > \varepsilon_u, \mathrm{SINR}_{u,kl}^{LE} > \varepsilon_0), & \text{For FD} - \text{ZFLE}, \ \forall \ l \\ 1 - p(\mathrm{SNR}_{u,n} > \varepsilon_u, \mathrm{SINR}_{u,kl}^{\mathrm{DFE}} > \varepsilon_0), & \text{For FD} - \text{DFE}, \ \forall \ l \end{cases}, \tag{40}$$

where $\varepsilon_u = 2^{R_{u,n}} - 1$ and $R_{u,n}$ denotes the adaptive-rate transmission, given as[4]

$$R_{u,n} \le \log\left(1 + \frac{\mathrm{SNR}|H_u[n, u-1]|^2}{\mathrm{SNR}|H_u[n, u-1]|^2 + 1}\right), \quad \text{for the } M'\text{th Us with low mobility.} \tag{41}$$

5 Theoretical Performance Analysis

This section aims to compare the performance of the proposed NOMA-OTFS and NOMA-OFDM schemes in an MU-MIMO VLC system with low latency by analyzing several key metrics, such as SE, BER, and PAPR. The performance of the NOMA-OTFS VLC scheme is primarily determined by power allocation γ_u, Therefore, to achieve a better performance, users in non-overlapping regions are typically allocated more power, whereas those in overlapping areas require less power. In our scenario, the optical signals received by NOMA users U_3 and U_4 in the overlapping region (sub-cell) are a result of signal superposition from two LEDs. These signals are decoded at the receiver using SIC processing, as shown in Fig. 4. The effect of the error propagation due to SIC decoding is particularly considered to achieve a more reliable expression of the SINR.

To minimize the SINR of the proposed NOMA-OTFS VLC system based on the regulated power allocation γ_u scenario, we apply an equalization approach that includes FD-ZFLE and DFE.

5.1 Theoretical Limits on BER

To mitigate this issue, the primary focus is on minimizing the BER of the proposed downlink MIMO-VLC-based NOMA-OTFS, which is obtained by applying the pairwise error probability (PEP) using the ML decision at the receiver by normalizing the elements of the noise matrix to variance one based on Eq. (18). The following equation represents this approach as[16,15]

$$\hat{S}_{\mathrm{ML}} = \arg \min_{S \in \mathbb{S}} \left(\frac{\mathcal{R}_p}{\sigma} \|HS\|^2 - 2H^T HS \right), \tag{42}$$

where $\mathbb{S}$ represents the set of all matrices that can be transmitted using NOMA-OTFS. Assuming that S_1 and S_2 are the two transmit signal matrices, PEP is expressed as the probability of deciding in favor of S_2, given that S_1 was transmitted:

$$\begin{aligned} \mathrm{PEP}(S_1 \rightarrow S_2 | H) &= P_r(S_1 \rightarrow S_2 | H) \\ &= P_r \left(y^T H(S_2 - S_1) > \frac{\mathcal{R}_p}{2\sigma} (\|HS_2\|^2 - \|HS_1\|^2) \right) \\ &= P_r \left(\frac{2\sigma}{\mathcal{R}_p} \eta_u^T H(S_2 - S_1) > \|H(S_2 - S_1)\|^2 \right). \end{aligned} \tag{43}$$

Let $z \triangleq \frac{2\sigma}{\mathcal{R}_p} \eta_u^T H(S_2 - S_1)$ denote the Gaussian random variable with variance $\mathrm{Var}(z) \triangleq \frac{4\sigma^2}{\mathcal{R}_p^2} \|H(S_2 - S_1)\|^2$ and its mean value be null. Then, the PEP expression is given as

$$\mathrm{PEP}(S_1 \rightarrow S_2 | H) = Q \left(\frac{\mathcal{R}_p}{2\sigma} \|H(S_2 - S_1)\| \right). \tag{44}$$

Therefore, the theoretical limits on BER for the ML estimator are bounded as

$$\begin{aligned} \mathrm{BER} &\leq \frac{1}{2NM} \mathrm{PEP}(S_1 \rightarrow S_2 | H) \frac{d(S_1, S_2)}{\Gamma} \\ \mathrm{BER} &\leq \frac{1}{2NM} Q \left(\frac{\mathcal{R}_p}{2\sigma} \|H(S_2 - S_1)\| \right) \frac{d(S_1, S_2)}{\Gamma}, \end{aligned} \tag{45}$$

where $d(S_1, S_2)$ denotes the correspondent Hamming distances and $\Gamma = \log_2(NM)$ bits per channel use (BPCU) is the achieved rate of the system.

5.2 Computation of the Achieved Sum Rate

As shown in Fig. 4, the SIC process is used in the final Us-NOMA stage to decode symbols transmitted via OTFS modulation for all Us-multiplexing. The data rate for the m'th subcarrier and u'th user in NOMA-OTFS is obtained from Eq. (41) using the following equation:

$$R_m^u = B_{w_m} \log_2(1 + \mathrm{SINR}_{u,kl}). \tag{46}$$

Therefore, based on Eq. (46), the sum data rate, denoted as R_{sum}, achieved by all users in NOMA-OTFS can be given as

$$R_{\mathrm{sum}} = \sum_{u=1}^{4} \sum_{m=0}^{M-1} R_m^u. \tag{47}$$

In actual applications, we are interested in seeing how practicable the designs are on actual user-experienced channels. To achieve this, we compute the SINR using an average optical power specification that considers the lighting requirements of VLC systems. In a conventional definition of SINR, overlapping signals and non-overlapping signals are parameterized in the same way.

Our proposed scenario uses the NOMA-OTFS algorithm to equalize the MIMO-VLC channel, which is listed in Algorithm 1. It provides a detailed description of the NOMA-OTFS technique that we employ in our proposed approach to equalize the MIMO-VLC channel. This approach is designed to achieve a trade-off between implementation complexity and detection performance.

NOMA-OTFS offers the advantage of reduced system complexity by avoiding the use of complicated OTFS modulation transforms. Recent research findings indicate that the minimum computational complexity of an OTFS detector is $\mathcal{O}(NM \log_2(N))$, in which each OTFS frame contains $NM(4)/N_C$ codes words, where N_C is the code length. In Algorithm 1, we investigate practical SIC schemes based on FD-ZF and FD-DFE Equalization. Consequently, the implementation of FD-ZFE-SIC and DFE-SIC involves a significant number of relatively complex

operations, such as matrix inversions, which grow exponentially with the number of users at the receiver.

As a result of Algorithm 1, the DFE equalizer emerges as an effective solution in indoor VLC scenarios with MU-MIMO configurations. However, it introduces additional complexity and feedback delay, which are sustained due to the minimal computational complexity of $\mathcal{O}(N^3 M^3)$. Nevertheless, the performance of DFE surpasses that of FD-ZFE and the minimum mean squared error (MMSE) equalization. Furthermore, the computational complexity of the MMSE-SIC detector is estimated to be $\mathcal{O}(NM \log_2(NM))$, similar to the computational complexity of the ZFE scheme.

6 Numerical Results and Discussion

In this section, we present the analytical and simulation results for various NOMA-OTFS scenarios. We used Monte Carlo simulations to analyze the BER, outage probability, SE, and PAPR for a 2×2-MIMO-VLC based on a downlink NOMA-OTFS system in an indoor room with four users. The parameters utilized in the system simulation are detailed in Table 1. Notably, the NOMA-OFDM benchmark scheme, integrating the scenario proposed by Refs. 13 and 17 and the optimal exhaustive searching technique, is proposed with the assumption of a perfect BER and lowest PAPR with a high SE performance using SIC equalization methods.

In Fig. 5, the SNR gain of the NOMA-OTFS scheme is illustrated for different receiver locations within the room where the two LEDs are positioned, as shown in Fig. 6. Notably, the SNR of NOMA-OTFS outperforms 20 dB at all locations in the room. Furthermore, users located near the LEDs experience a considerable increase in SNR, with values reaching up to 40 dB. These results suggest that the NOMA-OTFS scheme's spatial distribution is highly effective in improving VLC indoor room performance.

Figure 7 shows the BER performance of the proposed NOMA-OTFS and NOMA-OFDM schemes in an MU-MIMO VLC system. The BER is computed using both 4-QAM and 16-QAM order modulation schemes. It is assumed that each receiver has the same relative mobility and employs an MMSE equalizer. For a fair comparison, we apply an ML detection for OFDM channel coding, which is designed to exploit all possible interference. According to the results, we first note that the proposed NOMA-VLC system based on OTFS has a better BER compared with OFDM for various modulation schemes with different orders. On the other hand, for OTFS transmission, the variation in Doppler shifts caused by different user mobility profiles does not alter

Table 1 2×2-MIMO system simulation parameters for an NOMA-based OTFS downlink VLC.

Parameters	Values
Number of the LEDs, N_t	2
LED height	3 m
Semi-angle, $\phi_{1/2}$	70 deg
Modulation bandwidth, B_w	25 MHz
OTFS modulation order, M_{mod}	4-QAM, 16-QAM
Number of the PDs, N_r	4
Photoresponsivity, R_p	1 A/W
Photodiode area	1 cm^2
FOV	85 deg
Azimuth	0 deg
PD height	0.80 m
Number of subcarriers	256

(a) LEDs co-ordinates

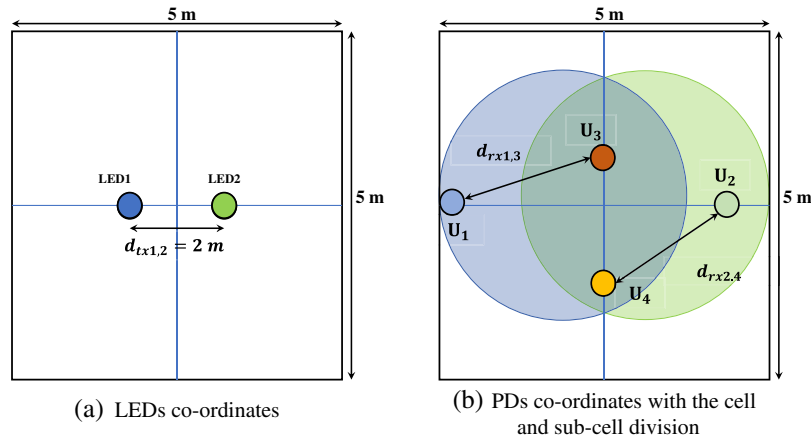(b) PDs co-ordinates with the cell and sub-cell division

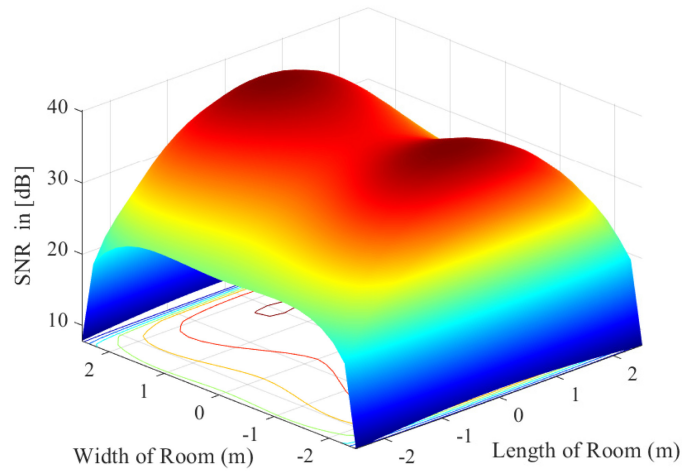**Fig. 5** Transceiver position (a) of the LEDs, (b) PDs, cell, and sub-cell division.

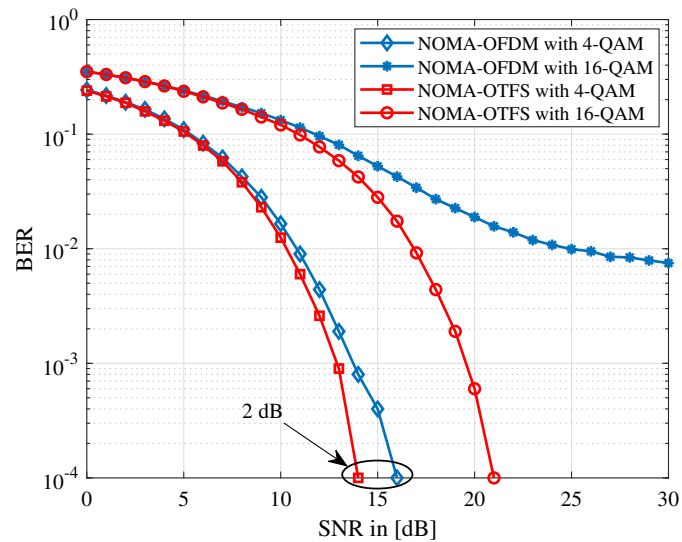**Fig. 6** Spatial distribution of SNR NOMA-OTFS for the indoor room VLC system.

Fig. 7 BER performance comparison for downlink NOMA users with OTFS and OFDM VLC versus SNR ($N = 8$, $M = 8$, 4-QAM, and 16-QAM).

the inherent 2D convolution nature of the signal-channel interaction in the DD domain. However, NOMA-OFDM requires accurate channel state information to perform interference cancellation and power allocation γ_u, which can be difficult to estimate in practice. At a BER of 10^{-2}, the proposed NOMA-OTFS system achieves an average SNR gain of almost 5 dB over the NOMA-OFDM. Specifically, for the 16-QAM modulation order, NOMA-OTFS delivers a gain of 7.3 dB over NOMA-OFDM at a BER of 10^{-2}. Furthermore, it can be observed that, with NOMA-VLC based on OTFS at a BER of 10^{-4}, we achieve a normalized SNR difference of 2 dB over NOMA-OFDM in the VLC noisy channel.

The usage of multiple Dopplers can be difficult to equalize and is determined by the sub-channel gains. This can represent a problem in high SNR conditions and affect the performance of NOMA-OFDM. The integration of OTFS modulation into NOMA VLC downlink systems can be a promising solution to the challenges of OFDM and can improve the transmission in the DD domain, as opposed to the TF domain. By leveraging the benefits of OTFS modulation, such as improved channel equalization and resistance to a Doppler shift, NOMA VLC systems can potentially achieve better SE and reliability, particularly in user-mobility scenarios.

The nonlinearity of the LED in a VLC system will have a significant impact on the transmission performance of NOMA-OFDM with a high PAPR. On the other hand, the downlink NOMA-OTFS multi-user VLC systems can reduce the PAPR while preserving high data throughput. The complementary cumulative distribution function (CCDF) of PAPR is analyzed for NOMA-OTFS modulation in VLC and is compared with the NOMA-based OFDM scenario.

Figure 8 shows the simulated CCDF of PAPR performance as a function of PAPR for our proposed downlink MU-2×2-MIMO VLC system with $M = 8$ and $N = 8$. We note a close resemblance between the simulated CCDF of NOMA-OTFS and its corresponding analytical CCDF. As shown in Fig. 8, the NOMA-OFDM has a high PAPR compared with the proposed NOMA-OTFS scheme. This difference in PAPR for downlink MU-VLC systems is attributed to the nonlinearity of the LEDs, which significantly impacts the performance of data transmission. It can be seen that the OTFS modulation reduces the PAPR to a certain extent.[6] However, the combination of the MIMO NOMA technique and the OTFS modulation, i.e., NOMA-OTFS, can significantly reduce the PAPR with low complexity. Furthermore, the results show that the CCDF of NOMA-OTFS decreases significantly, reaching a value of 10^{-4}. By contrast, the CCDF of NOMA-OFDM reduces only up to 10^{-2}. Comparing our proposed NOMA-OTFS scheme with NOMA-OFDM, we observe a notable reduction of 2.7 dB in the PAPR. These results indicate that the efficient design and use of NOMA-OTFS algorithms can significantly improve PAPR performance in multiple-user MIMO VLC systems.
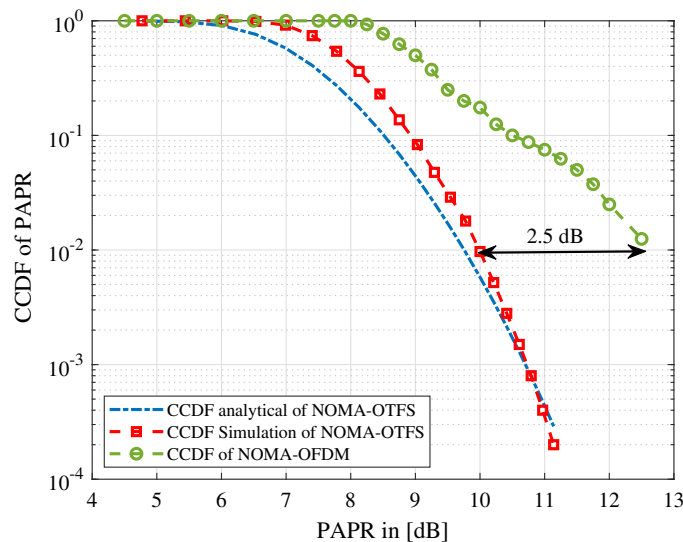

Fig. 8 CCDF of PAPR for NOMA-OTFS modulation in VLC and the comparison with the NOMA-based OFDM scenario.

Figure 9 shows the outage probabilities achieved by the 2×2 MIMO-VLC downlink systems using NOMA-OTFS and OMA-OTFS modulation techniques. The performance of NOMA-OTFS achieved by the DFE outperforms the FD-ZFLE in terms of outage probability. This improvement in performance can be attributed to the diversity of multi-path gain, which enables the DFE equalizer to mitigate the effects of fading and interference more effectively than the FD-ZFLE. The results demonstrate that the outage probability of NOMA-DFE is comparable to that of OMA-DFE, indicating that both techniques offer similar levels of error correction and signal quality. Moreover, the FD-ZFLE outage performance is dominated by the reliability of detection of OMA users' signals $x_u[N - 1, M - 1]$.

In NOMA systems, equalization plays a crucial role in mitigating the impact of inter-user interference. Figure 10 shows the BER performance of the FD-ZFLE and DFE-SIC equalizers compared with the MMSE-SIC equalizer described in Ref. 13 for the 2×4 MIMO-NOMA-OTFS VLC system.

The performance of DFE equalization in terms of the BER outperforms ZF and MMSE equalization in an MIMO-NOMA-OTFS VLC system. This is because DFE equalization utilizes feedback from previously detected symbols to cancel IUI and reduce ISI, resulting in an
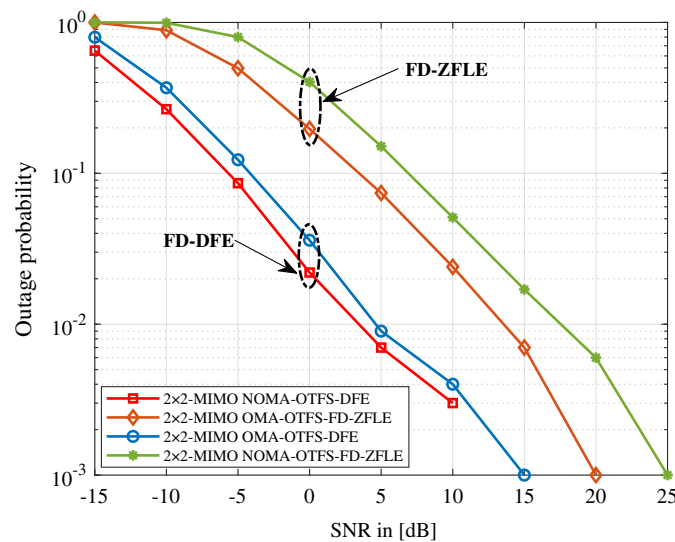

Fig. 9 Outage probability comparison of 4-Us 2×2-MIMOdownlink OTFS-OMA/NOMA VLC ($M = N = 8$).
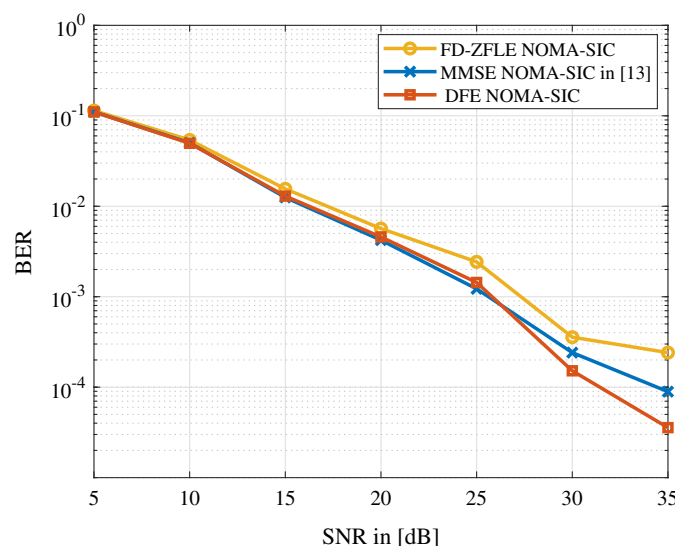

Fig. 10 BER performance of the DFE, FD-ZFLE, and MMSE-SIC equalizers versus the SNR.

improved BER performance. The ZF equalizer eliminates ISI by projecting the received signal onto the null space of the interference channel matrix. However, ZF equalization is prone to noise enhancement and can lead to amplification of noise at the receiver. The MMSE equalizer, on the other hand, considers the noise variance and the channel estimation error, resulting in a better performance than ZF equalization. The MMSE equalizer reduces the noise enhancement problem of the ZF equalizer and provides more robust performance in the presence of channel estimation errors, that is, because the interference is boosted by the amplified noise imposed by the H^+ matrix inversion. In Fig. 9, we demonstrate the performance DFE NOMA-SIC for each user, e.g., DFE equalizer gains up to 1.8 dB of BER $= 1.22 \times 10^{-3}$ compared with the FD-ZFLE approach. The observed performance gain can be attributed to the utilization of either the ML detector or the matched filtering matrix $H_u^H H_u$, which outperforms the performance of H_u at the receiver. Additionally, the MMSE-SIC initially estimated SNR of up to 25 dB, making it a more reliable choice for modulation orders such as 4-QAM. However, with the DFE, the BER performance is improved by around $\approx$4 dB at BER $= 10^{-4}$ compared with MMSE-SIC. Therefore, from Fig. 10, DFE has a better BER performance in the important SNR (E_b/N_0), when reaching the maximum value from a BER of 5×10^{-5} at 35 dB.

To evaluate the performance of our proposed NOMA-OTFS aided MU-MIMO VLC systems, we implemented a specific scenario. In this scenario, we divide the four users into two NOMA cells. As shown in Fig. 5, the location coordinates of LED are considered to be (1.5 m, 1.5 m, 3 m), and users U_1 and U_2 are specifically assigned to NOMA location cells with coordinates ($x_r = 2.5$ m, $y_r = 4$ m, $z_r = 0.8$ m) and ($x_r = 2.5$ m, $y_r = 4$ m, $z_r = 0.8$ m), respectively. On the other hand, users U_3 and U_4 are positioned at the intersection of these two cells with coordinates ($x_r = 2$ m, $y_r = 2.5$ m, $z_r = 0.8$ m) and ($x_r = 3.75$ m, $y_r = 2.5$ m, $z_r = 0.8$ m), as visually demonstrated in the figure. In this scenario, we utilized a symmetrical model in which both NOMA cells maintain an equal distance from the LEDs. In addition, each cell is assigned a distinct spreading code, implying that both cells possess their own unique codes. Furthermore, the four users are positioned at varying distances from the LEDs, $d_3 < d_4 < d_2 < d_1$, which are differentiated through SIC technique from PD-NOMA, resulting in different power levels for each user. This configuration allows us to analyze the system performance and assess the efficiency of our proposed NOMA-OTFS approach.

Figure 11 shows that the BER performance of 4-Us varies with the power allocation values of each user. To improve the users' BER, we give the different values $\gamma_1 = 0.29$, $\gamma_2 = 0.26$, $\gamma_3 = 0.21$, and $\gamma_4 = 0.24$ of allocation power for four users, respectively. As shown in Fig. 11, U_4 has a better BER compared with users U_3, U_1, and U_4, which is explained by the high-power allocation power factor $\gamma_4 > \gamma_3$. Moreover, U_1 and U_2 have similar BER curves and
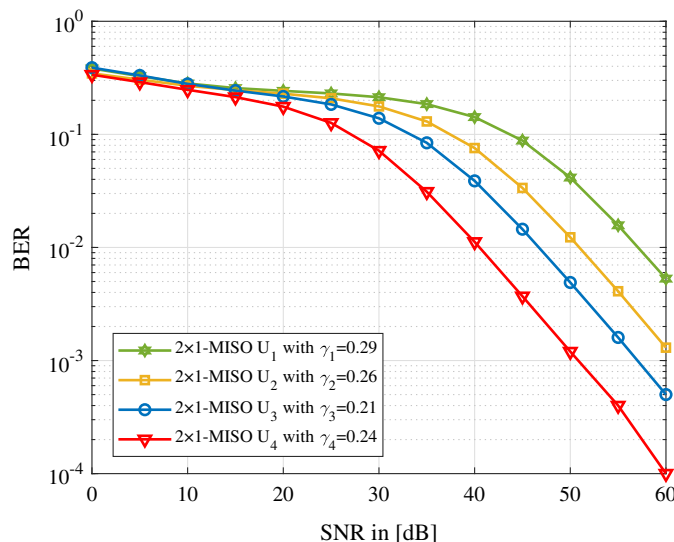

Fig. 11 BER performance of 4-Us MISO as a function of the SNR for the downlink VLC network proposed with the different power allocation coefficient values.

nearly coincide before 20 dB of SNR value. However, U_2 achieves a better performance compared with NOMA-user U_1 at a higher SNR. This is because both users receive an equal power level, but their respective distances from the transmitter's access points are slightly different. The average BER for overlapping users U_3 and U_4 is superior to that of U_1 and U_2, primarily due to the allocation power factors and varying distances between the users and the transmitter. This results in an average SNR gain of 10 dB at a BER of 10^{-2}.

Figure 12 shows the BER performance in a downlink 2×2-MIMO NOMA-OTFS VLC system with four users. It is worth noting that the power allocation coefficients remain unchanged. The results clearly illustrate the significant impact of the MIMO effect on the BER of all four users. Notably, as the SNR increases, a substantial decrease in the BER is consistently observed among all four users. Specifically, the distant users U_1 and U_2 experience a notable reduction in the BER, reaching a value of 3.4×10^{-4} at an SNR of 40 dB. Similarly, the nearby user U_3 and the middle user U_4 exhibit a substantial decrease in the BER, achieving a value of 10^{-4} at an SNR of 40 dB. By comparing the BER of four users in two scenarios, MIMO and MISO, in the NOMA VLC system utilizing OTFS modulation, it becomes apparent that the 2×2-MIMO system exhibits superior performance compared with the 2×1-MISO system.

In the following analysis, we evaluate the performance of our MIMO-VLC system by examining the impact of varying power allocation factors γ_u for each user U_u. We maintain the identical model presented in Fig. 5. We assign different power allocation factors to each user, with the values attributed as follows: $\gamma_1 = 0.33$, $\gamma_2 = 0.22$, $\gamma_3 = 0.15$, and $\gamma_4 = 0.30$ for four users U_1, U_2, U_3, and U_4, respectively. The BER performances of four users in the 2×2-MIMO VLC systems based on NOMA-OTFS are shown in Fig. 13, with respect to the SNR. It is evident that the BER for all users improves as the SNR increases.

The observed enhancement in the BER for middle user U_4, with a power allocation factor γ_4 of 0.30, as opposed to when $\gamma_4 = 0.24$, highlighting the impact of power allocation on the overall system performance. The higher power allocation U_4, as it is located at a greater distance, helps compensate for the effects of channel attenuation and interference. In our specific case, a notable gain of 5 dB is observed at a BER of 10^{-3}, signifying a substantial improvement in the quality and reliability of the received signal for user U_4. The BER of user U_4 is better than that of user U_3, and this can be attributed to the allocation of higher power to U_4 as it is a remote user and U_3 is not. This case $\gamma_4 = 0.30$ is not energy efficient because it requires more transmit power. As a near-user, U_3 receives a relatively lower power allocation, which has implications for its BER enhancement. Moreover, even though distance d_1 is greater than d_2, the BER performance of user U_1 is greater than that of user U_2. Giving more power allocation to U_1 compared with U_2 is useful to even out the impact of the difference distance between them. It can also be seen that the
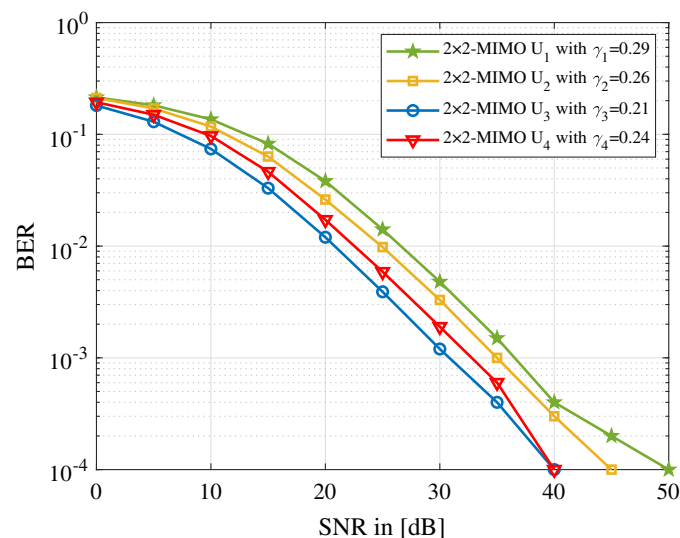

Fig. 12 BER performance of a 4-Us 2×2-MIMO system in the downlink VLC system with fixed power allocation coefficient values as a function of the SNR.
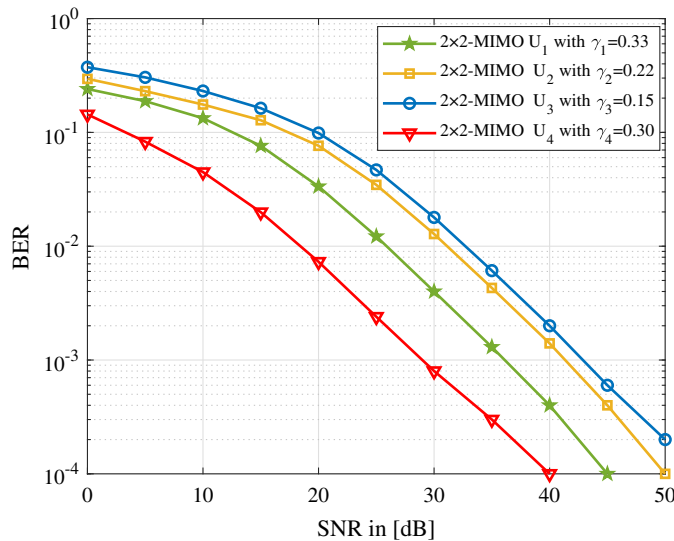
Fig. 13 BER performance of a 4-user 2×2-MIMO system in the downlink VLC network with various power allocation values as a function of the SNR.

performance of U_1 remains the same at a low SNR, which means that this user's γ_1 should be adjusted to the higher value due to its location. In multi-user NOMA scenarios, optimizing power allocation resources emerges as an essential factor in enhancing the performance of the BER in NOMA-based VLC systems. From the observations, it becomes evident that careful tuning of power allocation can potentially generate substantial benefits by improving the overall system performance.

Figure 14 presents a comparison of the spectral efficiency achieved by 2×2-MIMO VLC systems utilizing OTFS or OFDM modulation, along with either OMA or NOMA techniques. It is evident that our VLC proposal achieves a higher spectral efficiency compared with the benchmarking NOMA-OFDM approach. At a low SNR, the OMA-OTFS approximates to NOMA-OTFS, while satisfying the outage probability criterion of multi-users. In addition, we note that the performance advantage grows with the number of Us because of the higher freedom degree. At an SNR of 5 dB, the SE of the 2×2-MIMO NOMA-OTFS system exceeds
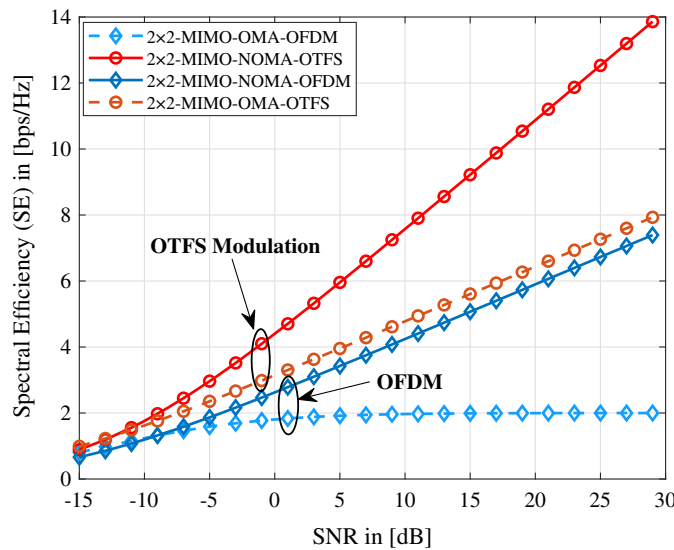

Fig. 14 Spectral efficiency as a function of the transmit SNR for two VLC scenarios OMA and NOMA using OFDM/OTFS modulation ($N = 8$, $M = 8$, $\gamma_1 = 0.29$, $\gamma_2 = 0.26$, $\gamma_3 = 0.21$, and $\gamma_4 = 0.24$).

that of the NOMA-OFDM combination by 4 bps/Hz. Furthermore, we observe a notable enhancement in the SE of NOMA-OTFS when compared with OMA-OTFS.

Specifically, the application of NOMA in the context of OTFS provides significant benefits for high-mobility users. By allocating their signals over many TF resources, NOMA improves the resolution of OTFS modulation and enhances the reliability of signal detection, even in the presence of temporal and frequency channel variations. Furthermore, the introduction of OTFS-NOMA ensures that low-mobility users are not marginalized in terms of bandwidth allocation. In conventional OTFS-OMA, the bandwidth resources are predominantly occupied by high-mobility users, limiting the available resources for low-mobility users. However, with OTFS-NOMA, low-mobility users are granted access to these bandwidth resources, leading to improved spectral efficiency and reduced latency. It is well known that NOMA with OFDM suffers from ISI due to the Doppler scenario. Therefore, based on our analysis, NOMA-OTFS demonstrates promising capabilities in mitigating the ISI issue associated with NOMA-OFDM.

The TF characteristics of OTFS provide improved resilience against Doppler effects, reducing the impact of ISI and enhancing the overall performance of the NOMA system. Furthermore, our research demonstrates that the implementation of proposed MIMO-OTFS-based NOMA VLC systems yields notable advantages over MIMO-OMA VLC systems, particularly in terms of capacity and data rates. Through comprehensive analysis, we evaluated the performance of the downlink NOMA-OTFS scheme in the MU-MIMO VLC system. We specifically focused on the power allocation of four users in the downlink NOMA-OTFS scheme. The obtained results, as shown in Figs. 9 and 14, clearly indicate that the NOMA-OTFS approach surpasses the traditional OMA-OTFS approach by up to 10% in terms of both outage probabilities and SE performance. Furthermore, our analysis reveals that NOMA-OTFS outperforms NOMA-OFDM by up to 57% in terms of SE. This substantial gain in SE highlights the significant advantage of NOMA-OTFS in achieving higher data rates and accommodating more users within a given bandwidth, surpassing the capabilities of NOMA-OFDM. However, in MU-NOMA scenarios, optimizing power allocation resources emerges as an essential factor in enhancing the performance of the BER in NOMA-based VLC systems.

The observations from our study strongly indicate that a meticulous adjustment of power allocation has the potential to yield significant benefits, leading to an enhancement in the overall system performance. In the proposed NOMA-OTFS technique, the choice between using FD-ZFLE or DFE for VLC channel equalization has important implications and calculates the post-equalization SINR. Although DFE offers a performance improvement over FD-ZFLE in terms of channel equalization, it comes at the expense of increased computational complexity. The DFE scheme requires the estimation and cancellation of the ISI, which involves more complex calculations than the simple linear equalization performed by FD-ZFLE.

7 Conclusion

This paper introduced a highly efficient NOMA-OTFS transmission scheme designed specifically for the MU-MIMO VLC system. The emergence of NOMA-OTFS as a high data-rate, secure, and energy-efficient downlink transmission technique for VLC systems has led to increased research on the associated communication protocols compared with NOMA-OFDM. Although the primary objective of this research was to achieve a reduction in PAPR and improve the BER with high spectral efficiency, it was essential to address the issue of ISI in the NOMA system. Hence, our proposed work confirmed the crucial stage of NOMA-SIC, which involved equalization using efficient equalization schemes, such as DFE, FD-ZFLE, and MMSE-SIC. The results indicate that the DFE with SIC performed better than other equalizers, achieving a lower outage probability and better BER. In addition, the theoretical BER values were validated, confirming the effectiveness of the optimized analytical algorithm for ML-based downlink NOMA-OTFS modulation. In addition, when users' mobility and the number of users were considered, the simulation findings indicate that the proposed hybrid NOMA-OTFS MIMO-VLC system outperformed the traditional NOMA-OFDM in downlink VLC systems. Regarding the BER performance of four users in two scenarios MIMO and MISO, in the NOMA VLC system utilizing OTFS modulation, it was apparent that the 2×2-MIMO system exhibited superior performance compared with the

2×1-MISO system. This performance difference can be attributed to various factors, including the power allocation factors γ_u assigned to each user U_u, which can significantly impact the overall system performance. Finally, the proof-of-concept simulation results support the suggested VLC system's efficiency in this study. They motivate future research into other potential MU-MIMO VLC designs on NOMA-OTFS, such as optimizing the resource allocation, enhancing the system capacity, or investigating advanced signal processing techniques to further improve the performance of MU-MIMO VLC systems. We will also develop an SIC receiver by integrating the turbo error correcting codes along with DFE equalization (i.e., low complexity) for users of the NOMA-OTFS scheme, which can increase the VLC system robustness to noise.

Code and Data Availability

All code and data that support the plots and findings in this paper are available from the corresponding authors upon reasonable request.

Acknowledgments

References

1. M. El Jbari and M. Moussaoui, "Efficient nM-PAWM hybrid modulation scheme for high data transmission in visible light communication system," *e-Prime-Adv. Electr. Eng. Electron. Energy* **2**, 100061 (2022).
2. M. El Jbari, M. Moussaoui, and N. Chahboun, "A review on visible light communication system for 5G," in *Int. Conf. Adv. Technol. for Hum.*, pp. 84–95, Springer International Publishing, Cham (2021).
3. H. Marcoux et al., "Multi-user techniques in visible light communications: a survey," in *Proc. Int. Conf. Adv. Commun. Syst. Inf. Secur. (ACOSIS)*, pp. 1–6 (2016).
4. H. Marshoud et al., "Optical non-orthogonal multiple access for visible light communication," *IEEE Wireless Commun.* **25**(2), 82–88 (2018).
5. S. S. Bawazir et al., "Multiple access for visible light communications: research challenges and future trends," *IEEE Access* **6**, 26167–26174 (2018).
6. R. Hadani et al., "Orthogonal time frequency space modulation," in *IEEE WCNC'2017*, pp. 1–6 (2017).
7. P. Raviteja, E. Viterbo, and Y. Hong, "OTFS performance on static multipath channels," *IEEE Wireless Commun. Lett.* **8**, 745–748 (2019).
8. Y. Liu et al., "Developing NOMA to next generation multiple access: future vision and research opportunities," *IEEE Wireless Commun.* **29**(6), 120–127 (2022).
9. P. Raviteja, K. T. Phan, and Y. Hong, "Embedded pilot-aided channel estimation for OTFS in delay-Doppler channels," *IEEE Trans. Veh. Technol.* **68**(5), 4906–4917 (2019).
10. B. C. Pandey et al., "Low complexity precoding and detection in multi-user massive MIMO OTFS downlink," *IEEE Trans. Veh. Technol.* **70**(5), 4389–4405 (2021).
11. Z. Ding et al., "OTFS-NOMA: an efficient approach for exploiting heterogeneous user mobility profiles," *IEEE Trans. Commun.* **67**(11), 7950–7965 (2019).
12. B. Lin et al., "Experimental demonstration of bidirectional NOMA-OFDMA visible light communications," *Opt. Express* **25**(4), 4348–4355 (2017).
13. A. Chatterjee et al., "Nonorthogonal multiple access with orthogonal time–frequency space signal transmission," *IEEE Syst. J.* **15**(1), 383–394 (2021).
14. M. El Jbari and M. Moussaoui, "The hybrid pulse amplitude width modulation scheme: high efficiency technique for dimmable VLC systems," *J. Opt. Commun.* **1** (2023).
15. T. Narasimhan et al., "Quad-LED OTFS modulation in indoor visible light communication systems," in *IEEE Global Commun. Conf. (GLOBECOM)*, Madrid, Spain, pp. 1–6 (2021).
16. P. Saxena and Y. H. Chung, "Performance analysis of a NOMA-VLC system with random user location," *ICT Express* **9**(3), 439–445 (2023).
17. X. Guo and Y. Luo, "Hybrid NOMA/OFDMA visible light communication system with coordinated multiple point transmission," *Opt. Express* **30**, 47404–47420 (2022).

Mohamed El Jbari is a PhD student in electrical, electronic, and telecommunication engineering at the Laboratory of Information and Communication Technology (LabTIC), Abdelmalek

Essaadi University, National School of Applied Sciences of Tangier (ENSAT), Morocco. He received his master's degree in telecommunication system engineering in 2018 and his bachelor's degree in electronics in 2014 from the Faculty of Sciences, Abdelmalek Essaadi University, Tetuan, Morocco, respectively. His current research interests include, visible light communication, optical wireless communication engineering, terahertz communication, digital signal processing, embedded electronic, and telecommunication systems.

Mohamed Moussaoui received his PhD from the University of Valenciennes et du Hainaut Cambrésis (UVHC), France, in 2005, with specialization in wireless communications and his HDR degree (Habilitation to supervise PhD students) from the University of Abdelmalek Essaadi in 2016. From 2002 to 2004, he worked as a teaching research assistant at the University of Valenciennes, France. In 2007, he joined the ENSAT, Abdelmalek Essaadi University, Morocco, as a research professor. From 2011 to 2014, he served as the head of the Engineering Program "Telecommunications Systems and Networks" at ENSA of Tangier. From 2018 to 2021, he served as the head of Information and Communication Systems Department at ENSA of Tangier. His research interests include wireless sensor network, terahertz communication, visible light communication, 5G, 6G, IoT, distance learning theories, and science diplomacy.